

16th CIRP Conference on Modeling of Machining Operations

Validation of Material Models for Machining Simulation Using Mechanical Properties of the Deformed Chip

Patxi Fernandez-Zelaia^{a*}, Shreyes N. Melkote^a

^a*George W. Woodruff School of Mechanical Engineering, Georgia Institute of Technology, Atlanta, Georgia 30332, USA*

* Corresponding author. Tel.: +1-404-894-0368; fax: +1-404-984-9342. E-mail address: pfz3@gatech.edu

Abstract

Finite element simulation of machining is increasingly popular in both industry and academia. Simulation accuracy is, in part, critically dependent on identification of the appropriate material constitutive laws. Calibration and validation of the laws is typically limited to using uniaxial flow stress data and/or machining outputs such as forces, temperatures, and chip morphology features. The spatial distribution of material state (i.e. microstructure, mechanical properties, residual stresses) of the machined chip, which encodes path-dependent process information, is seldom utilized for model validation. In this paper we explore a complimentary validation technique that compares model predictions against measured spherical nanoindentation stress-strain curves.

© 2017 The Authors. Published by Elsevier B.V. This is an open access article under the CC BY-NC-ND license (<http://creativecommons.org/licenses/by-nc-nd/4.0/>).

Peer-review under responsibility of the scientific committee of The 16th CIRP Conference on Modelling of Machining Operations

Keywords: machining, validation, nanoindentation, microstructure, Johnson-Cook

1. Introduction

Johnson-Cook (JC) class constitutive models are attractive as they capture phenomenological material behavior and are computationally inexpensive [1]. Besides predictions of common process outputs such as forces and temperatures, manufacturers also consider the effects of the process on the final component mechanical surface properties. In this work we seek to investigate a constitutive model validation methodology that assesses the efficacy of a JC model through predictions of the final chip constitutive properties. Enabling this work are modern instrumented spherical nanoindentation experiments that generate indentation stress-strain curves, which capture both elastic and post-elastic deformation behavior of the machined chip material.

The strategy for validating the machining simulations using constitutive properties of machined chips is as follows: (1) spherical nanoindentation of experimentally generated chips is

performed to extract the physical indentation stress-strain curves, (2) machining simulations are performed to emulate machining experiments and to predict the final material state of the chip, (3) FEA simulations of the chip indentation process, subject to corresponding pre-strains predicted from machining simulations, are performed to yield simulated chip indentation stress-strain curves, (4) the simulated indentation stress-strain curves, which are implicitly dependent on the machining constitutive model, cutting conditions, and the process history, are compared against the physical experiments.

2. Instrumented Spherical Nanoindentation

Traditional uniaxial mechanical testing techniques cannot be utilized to characterize the machined sub-surface or the machined chips. Therefore, indentation techniques are often used to measure the hardness of machined materials. Hardness measurements however provide an aggregate measure of the

material response; elastic and post-elastic behavior cannot be inferred from a hardness measurement. Instrumented indentation enables the measurement of the load-displacement history, which encodes the behavior of the material beneath the indenter, see Figure 1a.

Interpreting indentation results is made difficult by the highly multiaxial and graded deformation response beneath the indenter. Therefore, advanced post-processing methods are needed to interpret indentation experiments. Spherical indentation experiments are attractive since close-formed Hertzian mechanics solutions of the elastic deformation exist. A framework was developed around the Hertzian contact equations which yields indentation stress-strain expressions consistent with the Hertzian analytical solutions [3-7]. Note that the indentation stress-strain curve is only equivalent to uniaxial stress-strain curves in the elastic region. The mapping in the post-elastic regime is currently only known for simple cases such as elastic perfectly-plastic behavior for which the indentation stress saturates at $\sim 2\sigma_0$ [8]. The indentation stress-strain definitions are given as,

$$\sigma_{ind} = E_{eff}\epsilon_{ind} \quad \sigma_{ind} = P/\pi a^2 \quad \epsilon_{ind} = 4h_t/3\pi a \quad (1)$$

where σ_{ind} is the indentation stress, E_{eff} is the effective Hertzian modulus, ϵ_{ind} is the indentation strain, P is the measured indenter load, a is the measured contact radius, and h_t is the total prescribed indenter displacement. The contact radius can be inferred from continuous stiffness monitoring (CSM). A physical interpretation of these quantities considers an idealized compressed cylinder beneath the indenter, Figure 1b.

3. Experimental Methods

Orthogonal tube cutting experiments were performed on a Hardinge T-42 SP CNC lathe using oxygen free high conductivity (OFHC) copper. A single $0.1 \text{ mm}\cdot\text{rev}^{-1}$ feed was used along with three cutting speeds: 12, 20, 30 $\text{m}\cdot\text{min}^{-1}$. A 2mm tube wall thickness was used but preliminary cutting tests indicated that significant material side flow was present. Two concentric 1mm aluminum tubes were placed around the copper tube to constrain the slide flow and to ensure true plane strain cutting conditions. Tests were performed dry with 0° rake angle uncoated tungsten carbide inserts (Kennametal

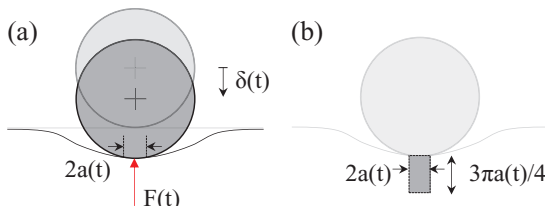


Figure 1. (a) Spherical indentation experiment prescribing a displacement and measuring force and contact radius, (b) the idealized compressed volume, and (c) multiaxial nodal displacements beneath a spherical indenter.

TCMW3251, KCK20) in the upsharp condition (cutting edge radius $\sim 10\mu\text{m}$).

Chips were prepared for imaging and nanoindentation using conventional mechanical polishing up to a $0.05\mu\text{m}$ colloidal silica suspension followed by electropolishing. Chips were exopy mounted to reveal the entire chip length in one direction

and the deformed chip thickness in the other. Electropolishing was done using Struer’s LectroPol with a phosphoric acid based electrolyte. The polished chips were imaged in a Tescan Mira XMH field emission SEM.

Nanoindentation was performed using an Agilent G200 Nanoindenter with CSM. A $100\mu\text{m}$ spherical indenter, estimated to yield a $\sim 10\mu\text{m}$ contact radius, was used. Arrays of 500nm depth indents were made in the middle of each chip with repetitions spanning the chip length.

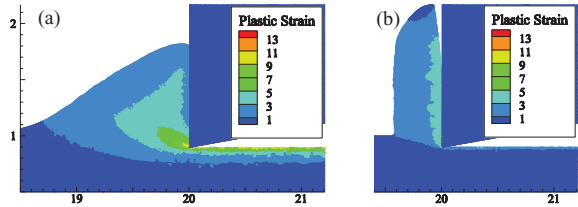


Figure 2. Machining simulations with $f=0.1\text{mm}\cdot\text{rev}$ and $V=12 \text{ m}\cdot\text{min}^{-1}$ (a) Johnson-Cook parameters [1] and, (b) Taylor impact parameters [2].

4. Numerical Methods

Plane strain simulations of the machining experiments were performed using ThirdWave Systems’ AdvantEdge software [9]. The JC [1] model was used to describe the OFHC Cu flow stress behavior. OFHC Cu model constants provided in the original JC paper prescribe a large strain-hardening exponent ($n=0.31$) which drives significant hardening producing an unrealistic chip morphology, as shown in Figure 2a. Instead model constants were taken from a study which calibrated the JC model to Taylor impact data that yielded a smaller hardening exponent ($n=0.0334$) [2]. We justify the use of the smaller value since it yields more realistic chip geometries, as shown in Figure 2b. The remaining constants are: strain rate constant $c = 0.009$, thermal softening exponent $m = 1.09$, initial yield $A = 90 \text{ MPa}$, and hardening slope $B = 340 \text{ MPa}$ [2].

Spherical nanoindentation simulations were performed in the commercial FE package Abaqus v6.16 [10]. The machined chip material state is transferred to indentation simulations through the use of a pre-strain. The indentation flow rule is the quasi-static JC model,

$$\sigma = A + B(\bar{\epsilon}_{pl} + \bar{\epsilon}_{pl,o})^n \quad (2)$$

where the A , B , and n , are identical to the values utilized in machining simulations. $\bar{\epsilon}_{pl,o}$ is the chip pre-strain prior to indentation and is equal to the effective plastic strain predicted from machining simulations. $\bar{\epsilon}_{pl}$ is the accumulated plastic strain due to indentation.

Note that the above flow law is equivalent to the quasi-static low temperature JC model. In this way, we guarantee the same assumed flow law governs material behavior across both the machining and indentation simulations and that the material state effects are transferred via the equivalent plastic strain.

Table 1. Machining simulation results in the middle of the chip.

ϵ_{pl}	$V = 12 \text{ m}\cdot\text{min}^{-1}$		$V = 20 \text{ m}\cdot\text{min}^{-1}$		$V = 30 \text{ m}\cdot\text{min}^{-1}$	
	σ_{11} (MPa)	σ_{22} (MPa)	ϵ_{pl}	σ_{11} (MPa) σ_{22} (MPa)	ϵ_{pl}	σ_{11} (MPa) σ_{22} (MPa)
2.39	-81.1	12.6	2.39	-103.0 26.4	3.17	-154.1 47.0

Download English Version:

<https://daneshyari.com/en/article/5470307>

Download Persian Version:

<https://daneshyari.com/article/5470307>

[Daneshyari.com](https://daneshyari.com)